SINAYA
A Philippine Journal for Senior High School Teachers and Students

Science and Technology

Percolation-Modeling Comparison Between the Conductivities of Zinc-Graphene Quantum Dot Nanocomposite and Graphite During Extracellular Electron Transfer in Microbial Fuel Cell Electrodes

Jamme Omar A. Biscocho
Ralph Calvin D. Almazan
Francis M. Emralino
Michelle T. Manglicmot

Philippine Science High School – CALABARZON Region Campus, Batangas City

Abstract: While promising as an energy production alternative through its sustainability and wastewater treatment utility, a microbial fuel cell is not widely used due to its low power output and high cost. The development of advanced electrode materials is currently being pursued to solve this problem. A zinc-graphene quantum dot nanocomposite was modeled using percolation theory as a prospective advanced electrode material. During extracellular electron transfer, the electrical conductivity properties of the material were studied through cellular percolation models, percolation probability functions, and electrical conductivity curves. These models were compared against those of the conventional graphite electrodes and the leading graphene electrodes. The nanocomposite was found to conduct at low probabilities of open sites and exhibit the highest electrical conductivity of the three materials for the longest duration across the interval. Based on the models, Zn-GQD was demonstrated to be an ideal MFC electrode material for its balance between the early onset of conduction and decently high electrical conductivity.

Keywords: percolation; Zn-GQD nanocomposite; microbial fuel cell; electrode materials; electrical conductivity

INTRODUCTION

Microbial fuel cells (MFCs) are electrochemical cells that generate electricity from organic matter through redox reactions of bacterial metabolism. They demonstrate promising performance in terms of versatility, simplicity, sustainability, and cleanliness of energy production and wastewater treatment utility (Do et al., 2018). However, industrial applications of MFCs are discouraged due to low electricity production, peaking at 36.9 milliwatts (mW), and high cost (Santoro et al., 2019). Fortunately, an improved understanding of the extracellular electron transfer mechanisms of bacteria revealed that developing advanced electrode materials can drastically magnify power outputs while minimizing costs (Slate et al., 2018).

The ideal MFC electrode exhibits excellent biocompatibility and good conductivity. Excellent biocompatibility promotes bacterial colonization and attachment, while good conductivity allows for the efficient transfer of electrons to generate higher electrical currents (Slate et al., 2018). The main candidates for electrode materials include metals and carbon-based materials. Metal electrodes display high conductivity but are incompatible with bacteria. Conversely, carbon-based electrodes show limited conductivity but allow convenient adherence of bacteria. Due to their inherent biocompatibility, carbon-based materials such as graphite are primarily used for MFC electrodes (Li et al., 2016).

Based on these criteria, the zinc-graphene quantum dot (Zn-GQD) nanocomposite is potentially an excellent prospect as an advanced electrode material. The nanocomposite has the biocompatibility of carbon-based materials through the GQD layer, with the natural conductivity of zinc metals augmented by the increased electron mobility from the aromaticity and quantum confinement exhibited by GQDs (Wang et al., 2016; Wu et al., 2013).

Computationally, these properties of Zn-GQD can be explored through percolation theory. Percolation theory deals with how initially unlinked points in a system form clusters or connections to link their opposite boundaries together (Stauffer & Aharony, 2018). In the context of MFC operation, the boundaries to be linked refer to the electrode-bacteria interface during the extracellular transfer of electrons from bacteria to the MFC electrodes.

Hence, the study sought to investigate the electrical conductivity properties of Zn-GQD electrodes by building percolation models such as cellular percolation models, percolation probability functions, and electrical conductivity curves to establish its application as an advanced electrode material for MFCs, the performance of these Zn-GQD models were compared to those of graphite and graphene—currently the widely used and the best MFC electrodes respectively (Li et al., 2016).

METHODOLOGY

Percolation Modeling of Zn-GQD Nanocomposite and Graphite

The cellular percolation models and percolation probability functions were developed using Wolfram Mathematica and Microsoft Excel. A program adapted from Wolfram (2011) was operated to determine the cellular percolation models using the inputted and the critical percolation thresholds of the Zn-GQD nanocomposite, graphite, and graphene for reference. The program of Wolfram (2011) was chosen for its feature of allowing users to interact with the visual output without touching the input code and its open content license. The models were devised to show how the electrical conductivity of each material evolves before and after reaching their respective critical percolation thresholds. Electrical conductivity manifests in the models at the instance when the percolating cells have a critical level of association.

The cellular percolation model was initialized on a block or square grid (Figure 1). Random cells in the block were opened and marked blue. Closed cells were marked white, and red cells in the lattice correspond to percolating cells, while blue and white cells correspond to open and closed cells, respectively. The program randomly selected the percolating cells from the open cells based on the estimated percolation threshold.

Figure 1

Cellular Percolation Model

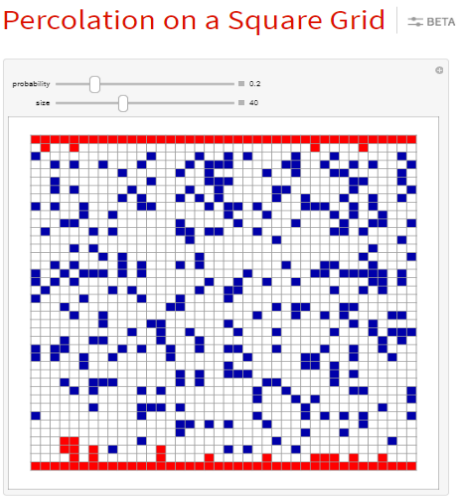

Note. From *Percolation on a Square Grid*, by S. Wolfram, 2011, Wolfram Demonstrations Project (https://demonstrations.wolfram.com/PercolationOnASquareGrid/). CC BY-NC-SA.

The modified parameters of the Mathematica program were as follows. The models were constructed from a square lattice with a 10-by-10 grid size which was the media for the percolating system. A 10-by-10 grid size was deemed appropriate after the following preliminary calibrations on the program. The researchers determined that sizes smaller than a 10-by-10 grid could not trace a $\theta(p)$-graph that assumes behavior consistent with literature. On the other hand, sizes larger than a 10-by-10 grid were consistent with the critical behavior of percolation at p_c, but did not form spanning clusters at p_c.

The topmost and bottommost rows of cells in the lattice serve as the percolation boundaries of the models. Eighty (80) individual cells in between the percolation boundaries served the percolation sites of the lattice. The program utilized probability values as its input to calculate the values of the percolation probability function $\theta(p)$ concerning the adapted percolation thresholds for graphene (0.6970402), Zn-GQD (0.199256), and graphite (0.3701) (Jacobsen, 2014; Lorenz et al., 2000; van der Marck, 1999).

The arguments of its SeedRandom[] function were modified to change the program's default critical threshold settings. This method was discovered while the researchers were studying the program of Wolfram (2011). The appropriate argument for each material was determined by initializing a variable for the argument in the SeedRandom[] function and appending the variable to the AutoRunSequencing() function slider. The minimum and maximum values for the AutoRunSequencing() function were modified to accommodate the range of argument values from 0 to 100 000. Afterward, the program sequence was operated using the AutoRun() function until the right argument was reached. For each material, the right argument was reached when a spanning cluster allowing information to percolate or flow from the topmost to the bottom layers

of the lattices and vice versa was first formed when p was set to their respective p_c-values. The arguments were 2912, 104, and 99 980 for Zn-GQD, graphite, and graphene, respectively.

Using Microsoft Excel, $\theta(p)$ for each material was graphically represented by plotting the results of the number of open cells divided by the total number of cells (80) concerning its corresponding p-value. Thirty (30) data points were plotted at 1/30-intervals for p by tabulating p and its corresponding $\theta(p)$ and graphing them using scatterplot. Thirty (30) values were chosen to align with the selected D_{crit} value for the statistical treatment. $\theta(p)$ had a domain of $0 \leq p_c \leq 1$. The calculated percolation probability values ranged from $0 \leq \theta(p_c) \leq 1$. The domain and range intervals were aligned with the 0-to-1 range of values for statistical probabilities (Bluman, 2018).

Plotting of Electrical Conductivity Curves

The electrical conductivity curves were developed in Microsoft Excel. The plot of the percolation probability function was converted to the percolating system's electrical conductivity plot through the classical percolation scaling equation (Eq. 3.1), where $\sigma(p)$ is electrical conductivity; σ_0 is the scaling factor; p is a probability parameter; p_c is the critical percolation threshold of the material; and T is the percolation exponent related to the structure of the material (Liu et al., 2017). The quantities used for the calculation of $\sigma(p)$ for the three materials are summarized in Table 3.1. The scaling factors used were based on the electrical conductivities exhibited by each material (Liu et al., 2017).

$$\sigma(p) = \sigma_0(p - p_c)^T \qquad \textbf{Eq. 3.1}$$

Values for p and its corresponding $\sigma(p)$-outputs were tabulated for each material. $\sigma(p)$ was graphically represented concerning probability using scatterplot. The constructed graph was used to visualize how the electrical conductivity of the percolating system evolved concerning

probability based on its critical percolation threshold. Thirty (30) data points were plotted by graphing at 1/30-intervals for p to be consistent with the 30 data points used in $\theta(p)$, which served as the reference for the scaling of $\sigma(p)$.

Table 1

Summary of quantities used for calculating σ(p) for Zn-GQD, graphene, and graphite

Material	σ_0	p_c	T
Zn-GQD	1.69 x 10^5 S/cm (Helmenstine, 2019; Protich et al., 2016)	0.199256 (Lorenz et al., 2000)	2.00 (Mutiso & Winey, 2012)
Graphene	1.00 x 10^6 S/cm (Mutlay & Tudoran, 2014)	0.6970402 (Jacobsen, 2014)	1.33 (Mutiso & Winey, 2012)
Graphite	1.33 x 10^4 S/cm (Bhattacharya et al., 2009)	0.3701 (van der Marck, 1999)	2.00 (Mutiso & Winey, 2012)

Data Analysis

Kolmogorov–Smirnov (KS) test was used to compare the $\sigma(p)$ curves of the Zn-GQD nanocomposite and the graphite electrodes. There were two sets of 30 electrical conductivity values at a probability of opening a site for each material. The continuous distribution of these samples satisfied the requirements for the KS test. KS test provides a means of testing whether a set of observations, a curve, or a continuous distribution significantly differs from another specified continuous distribution (Lilliefors, 2017).

The hypotheses for the KS test for the difference between the electrical conductivity curves of the Zn-GQD nanocomposite and the graphite electrodes were as follows:

1. H_0: There is no significant difference between the electrical conductivity vs. time curve plots of the Zn-GQD nanocomposite and the graphite electrodes.
2. H_1: There is a significant difference between the electrical conductivity vs. time curve plots of the Zn-GQD nanocomposite and the graphite electrodes.

The sample KS-statistic (D) was computed using Eq. 3.2, where D is the maximum vertical distance between two parallel $\sigma_{Zn-GQD}(p)$ and $\sigma_{Graphite}(p)$ values on the curve. The tabular KS-statistic (D_{crit}) was equal to 0.2417 for a sample size equal to 30 at a 95% confidence level. H_0 was rejected for $D > D_{crit}$ (Lilliefors, 2017).

$$D = |Maximum\left(\sigma_{Zn-GQD}(p) - \sigma_{Graphite}(p)\right)| \qquad \textbf{Eq. 3.2}$$

The statistical test was performed in Maxima. Maxima was used for its seamless accommodation of texts and mathematical symbols. These features enabled the neat presentation of textual documentation and mathematical computations.

RESULTS

Cellular Percolation Models

The cellular percolation models for Zn-GQD, graphene, and graphite are shown in Figures 2, 3, and 4, respectively. Two models for each figure are presented to show percolation when the independent variable, *p,* is less than, and when *p*is equal to the critical percolation threshold, p_c.

Figure 2

Cellular percolation models of Zn-GQD. (a) shows percolation at $p < p_c$. (b) shows percolation at $p = p_c$.

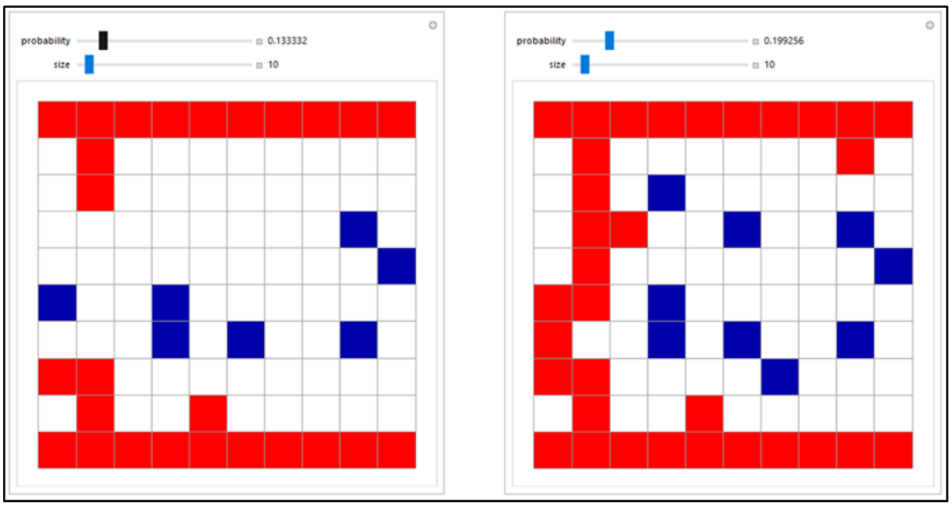

Note. Adapted from *Percolation on a Square Grid*, by S. Wolfram, 2011, Wolfram Demonstrations Project (https://demonstrations.wolfram.com/PercolationOnASquareGrid/). CC BY-NC-SA.

Figure 2 (a) shows the cellular percolation model of Zn-GQD at $p = 0.133333 < p_c$. At this probability level, a relatively small number of cells were either actively percolating or merely open. There were six actively percolating cells and seven open cells on the square lattice at random locations. The boundaries were still unlinked. Thus, no information could pass through the percolating system from boundary to boundary.

Figure 2 (b) shows the cellular percolation model of Zn-GQD at its critical percolation threshold, $p = 0.199256 = p_c$. At this probability level, a significantly greater number of cells were either actively percolating or merely open. There were 13 actively percolating cells and nine open cells at different cell locations on the lattice. The boundaries of the percolating system were now linked for the first time. A path involving the first two columns from the left paved the way for information to pass through from boundary to boundary.

Comparing Figures 2 (a) and 2 (b), there appears to be a sudden increase in the number of percolating cells when p is right before and right at p_c. The number of percolating cells increased from 6 to 13 when p rose from 0.133333 to 0.199256. This change demonstrated an increase of 216.67% in the number of percolating cells.

Figure 3

Cellular percolation models of graphene. (a) shows percolation at $p < p_c$. (b) shows percolation at $p = p_c$.

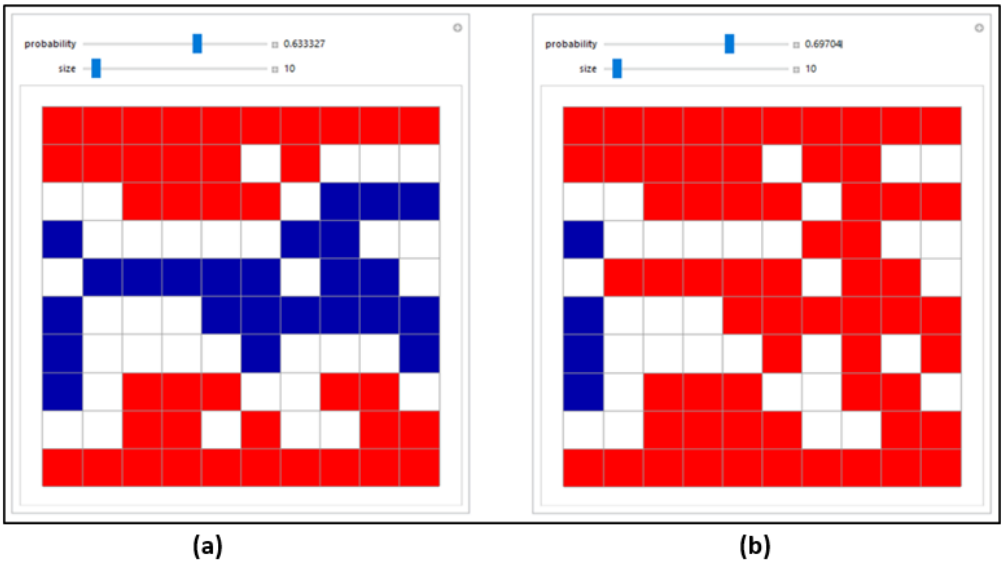

Note. Adapted from *Percolation on a Square Grid*, by S. Wolfram, 2011, Wolfram Demonstrations Project (https://demonstrations.wolfram.com/PercolationOnASquareGrid/). CC BY-NC-SA.

Figure 3 (a) shows the cellular percolation model of graphene at $p = 0.633327 < p_c$. At this probability level, a relatively large number of cells were either actively percolating or merely open. There were 20 actively percolating cells and 24 open cells at random locations on the square lattice. The boundaries were still unlinked. Thus, no information could pass through the percolating system from boundary to boundary.

Figure 3 (b) shows the cellular percolation model of graphene at its critical percolation threshold, $p = 0.6970402 = p_c$. At this probability level, a significantly greater number of cells were either actively percolating or merely open. There were 43 actively percolating cells and four open cells at different cell locations on the lattice. The boundaries of the percolating system were now linked for the first time. A path involving the second and third columns from the right paved the way for information to pass through from boundary to boundary.

When comparing Figures 3 (a) and 3 (b) side by side, there appears to be a sudden increase in the number of percolating cells when p is right before and right at p_c. The number of percolating cells increased from 20 to 43 when p rose from 0.133333 to 0.199256. This change demonstrated an increase of 215.00% in the number of percolating cells.

Figure 4

Cellular percolation models of graphite. (a) shows percolation at $p < p_c$. (b) shows percolation at $p = p_c$.

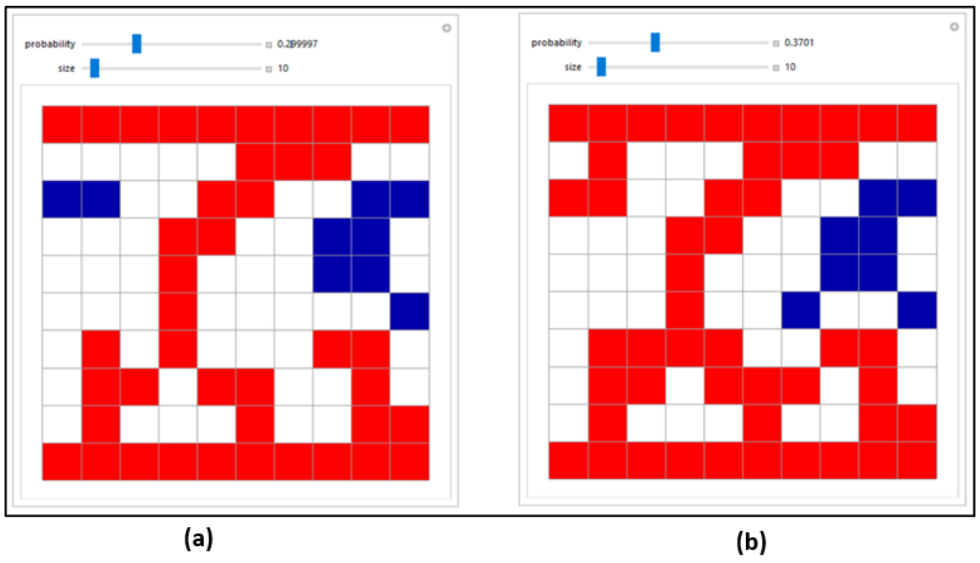

Note. Adapted from *Percolation on a Square Grid*, by S. Wolfram, 2011, Wolfram Demonstrations Project (https://demonstrations.wolfram.com/PercolationOnASquareGrid/). CC BY-NC-SA.

Figure 4 shows the cellular percolation model of graphene at $p = 0.29997 < p_c$. At this probability level, a relatively large number of cells were either actively percolating or merely open. There were 22 actively percolating cells and nine open cells on the square lattice at random locations. The boundaries were still unlinked. Thus, no information could pass through the percolating system from boundary to boundary.

Figure 4 (b) shows the cellular percolation model of graphene at its critical percolation threshold, $p = 0.6970402 = p_c$. At this probability level, a significantly greater number of cells were either actively percolating or merely open. There were 28 actively percolating cells and eight open cells at different cell locations on the lattice. The boundaries of the percolating system were now linked for the first time. A path involving the second to the fifth columns from the left paved the way for information to pass through from boundary to boundary.

When comparing Figures 4 (a) and 4 (b) side by side, there appears to be a significant increase in the number of percolating cells when p is right before and right at p_c. The number of percolating cells increased from 22 to 28 when p rose from 0.133333 to 0.199256. This change demonstrated an increase of 127.27% in the number of percolating cells.

Comparing the cellular models of each material, it appears graphene exhibited the most abrupt and abundant increase in the number of percolating cells, followed by Zn-GQD and then by graphite at the transition to their respective critical percolation thresholds. Furthermore, graphene possessed the highest number of percolating cells at the critical percolation threshold among the three materials. This material was followed by graphite and finally by Zn-GQD, with the least number of percolating cells at the critical percolation threshold. Consequently, the Zn-GQD material has the highest number of closed cells in the critical percolation threshold, followed by graphite and graphene.

Percolation Probability Functions

The comparison between the percolation behaviors of Zn-GQD, graphene, and graphite is elaborated by their $\theta(p)$ graphs shown in Figure 5.

Figure 5

Comparison of percolation probability functions between the three percolating systems

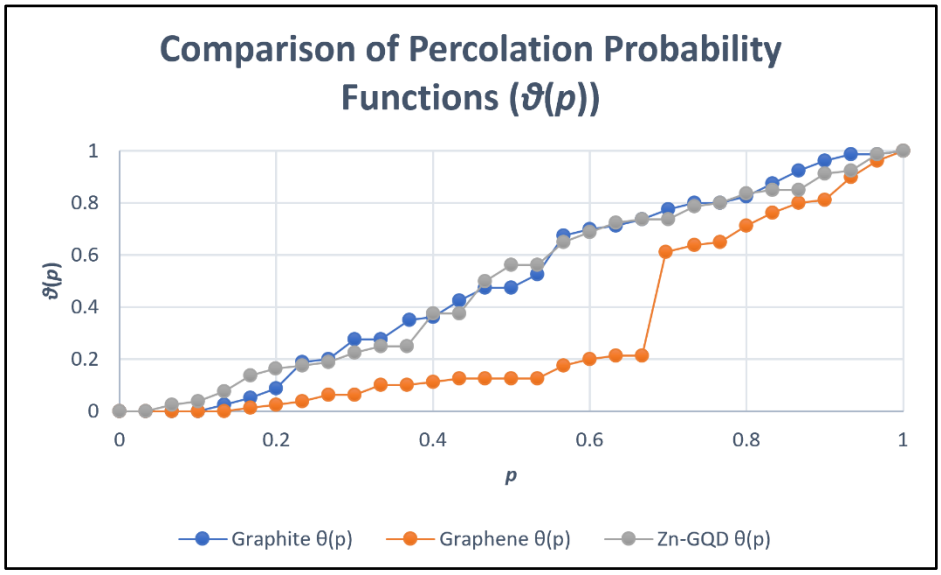

Based on Figure 5, the evolution of percolation probability functions of Zn-GQD and graphite was relatively similar compared to graphene. The Zn-GQD material had a percolation probability value of $\theta(p) = 0.1625$ at its critical percolation threshold, p = 0.199256. In contrast, the graphite material had a percolation probability value of $\theta(p) = 0.35$ at its critical percolation threshold, $p = 0.3701$. Both Zn-GQD and graphite reached their critical percolation thresholds earlier than graphene, which had a critical percolation threshold at $p = 0.69704$.

The percolation probability value of the Zn-GQD and graphite materials increased from $\theta(p) = 0.1375$ to $\theta(p) = 0.1625$ and from $\theta(p) = 0.275$ to $\theta(p) = 0.35$, respectively at their critical

percolation thresholds. The percolation probability of these two materials increased in a lower magnitude than graphene, whose percolation probability abruptly increased from $\theta(p) = 0.2125$ to $\theta(p) = 0.6125$ at its critical percolation threshold. These are reflected by the steeper slope of the percolation probability function of graphene compared to the plots of Zn-GQD and graphite at their respective critical percolation thresholds in Figure 5.Furthermore, their plots showed that the percolation probability functions of Zn-GQD and graphite increased more steadily than graphene.

Electrical Conductivity Curves

Figure 6

Plot of the electrical conductivity curve of Zn-GQD

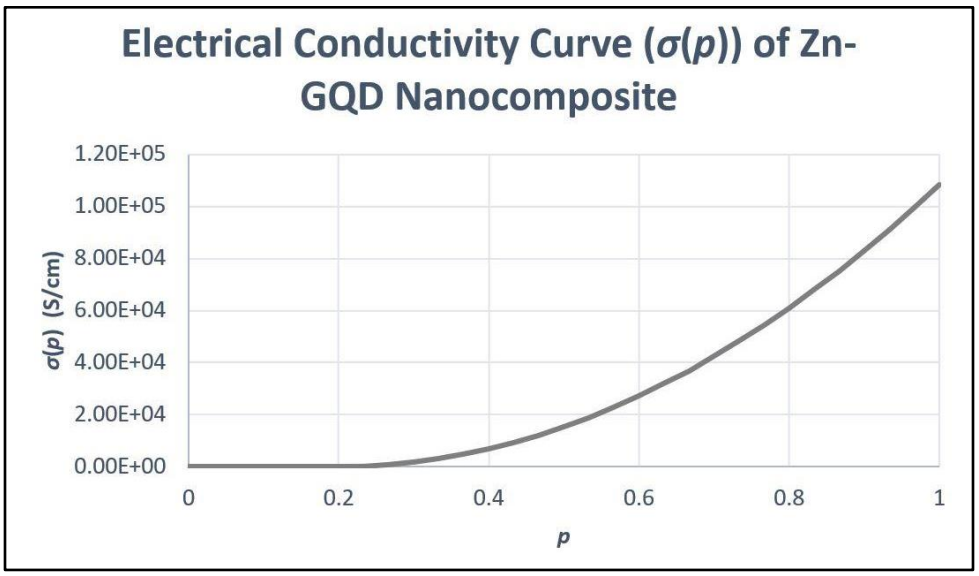

The electrical conductivity curve of Zn-GQD was described by Eq. 4.1. The Zn-GQD electrode started conducting at its critical percolation value, p_c. Below and at this value, the electrical conductivity of Zn-GQD was 0 S/cm. Above p_c, the electrical conductivity exponentially increased (Figure 6). The rate of increase was quadratic, as supported by the exponent in Eq. 4.1.

$$\sigma(p) = 1.69\, x\, 10^5\, S/cm\, (p - 0.199256)^{2.00} \qquad \text{Eq. 4.1.}$$

The electrical conductivity of Zn-GQD peaked at 1.08 x 10^5 S/cm. The peak was reached when p = 1, where all the cells in the square lattice were now percolating.

Figure 7

Plot of the electrical conductivity curve of graphene

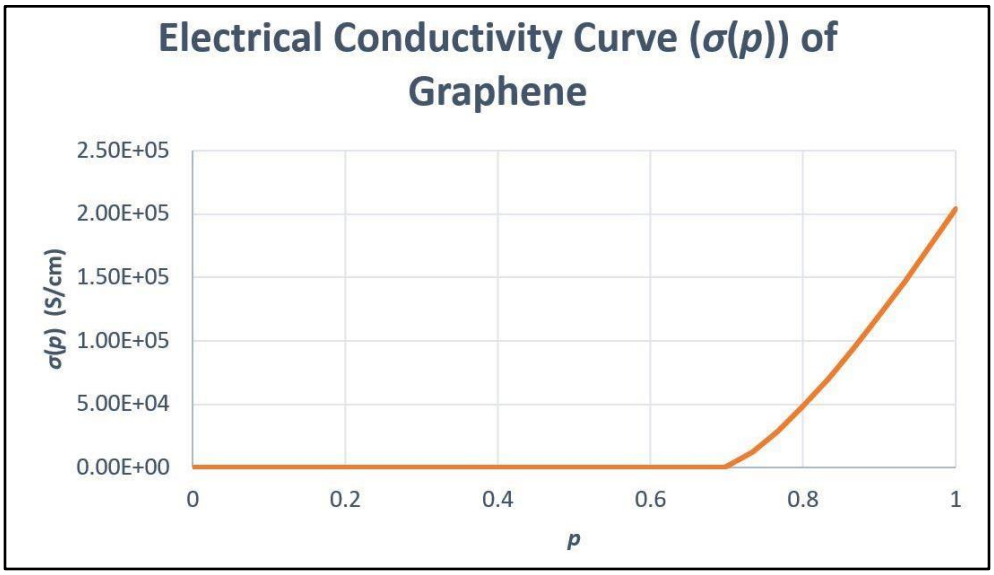

The electrical conductivity curve of graphene was described by Eq. 4.2. The Zn-GQD electrode started conducting at its critical percolation value, p_c. Below and at this value, the electrical conductivity of Zn-GQD was 0 S/cm. Above p_c, the electrical conductivity exponentially increased (Figure 7). The rate of increase was quadratic, as supported by Eq. 4.2.

$$\sigma(p) = 1.00\, x\, 10^6\, S/cm\, (p - 0.6970402)^{1.33} \qquad \text{Eq. 4.2}$$

The electrical conductivity of graphene peaked at 2.05 x 10^5 S/cm. The peak was reached when p = 1, where all the cells in the lattice were now percolating.

Figure 8

Plot of the electrical conductivity curve of graphite

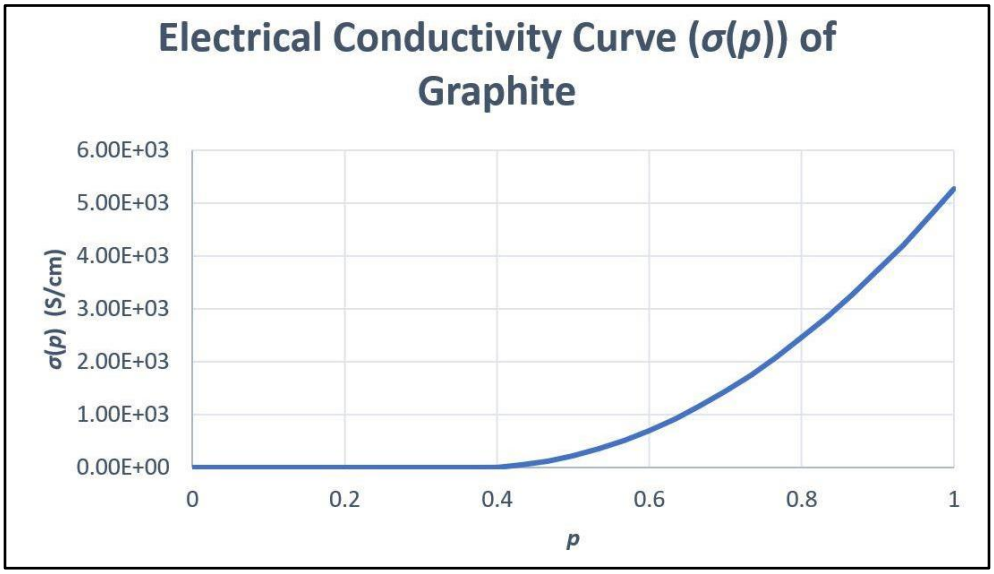

The electrical conductivity curve of graphite was described by Eq. 4.3. The Zn-GQD electrode started conducting at its critical percolation value, p_c. Below and at this value, the electrical conductivity of Zn-GQD was 0 S/cm. Above p_c, the electrical conductivity exponentially increased (Figure 8). The rate of increase was quadratic, as supported by Eq. 4.3.

$$\sigma(p) = 1.33\, x\, 10^4\, S/cm\, (p - 0.3701)^{2.00} \qquad \text{Eq. 4.3}$$

The electrical conductivity of graphite peaked at 5.28 x 10^3 S/cm. The peak was reached when p = 1, where all the cells in the lattice are now percolating.

Comparing the graphs of all three materials, they similarly showed a 0 value of electrical conductivity when $p \leq p_c$ (Figure 9). Furthermore, all of the curves, except for that of graphene, were similar in shape. The shape of curves for Zn-GQD and graphite were both quadratic when $p \geq p_c$ (Eq. 4.1 and 4.3).

Figure 9

Comparison of electrical conductivity curves between the three materials

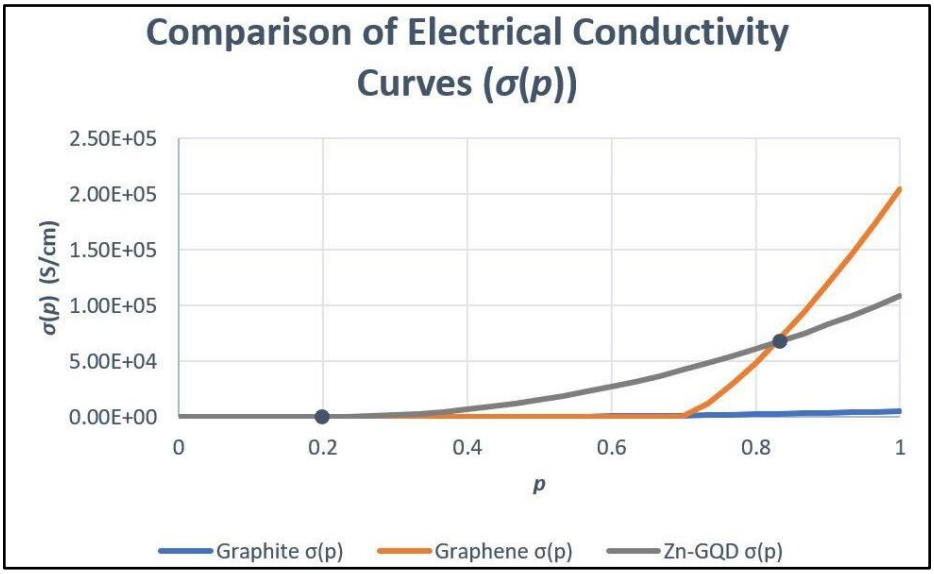

The curves differed in terms of the onset of conductivity, the rate at which conductivity increased, and the magnitude of conductivity. Zn-GQD was conducted the earliest, followed by graphite and then graphene. Zn-GQD was conducted 1.86 times earlier than graphite and 3.50 times earlier than graphene. Based on their graphs, graphene showed the sharpest rate of increase in electrical conductivity, followed by Zn-GQD and graphite. At different points, different materials were conducting the best. Zn-GQD was consistently the highest at $0.199256 < p < 0.828$. While graphene was consistently the highest at $0.828 < p \leq 1$. On the other hand, graphite consistently performed poorly compared to the other electrode materials. Graphene demonstrated the highest conductivity at its peak, followed by Zn-GQD and graphite. While Zn-GQD was 20.5 times more conductive than graphite, Zn-GQD was 1.89 times less conductive than graphene at maximum conductivity (Figure 9).

Statistical Treatment

Table 2

Significant difference between the electrical conductivity (σ(p)) curve plots of the Zn-GQD nanocomposite and Graphite

D	D_{crit}	Decision
103084.176814584	0.2417	Reject H_0

According to the difference between the maximum vertical distances of the electrical conductivities of Zn-GQD and graphite taken from their electrical conductivity values at $p = 1$, the computed KS-statistic (D) is greater than the tabular KS-statistic (D_{crit}). Hence, the null hypothesis is rejected, and there is a significant difference between the electrical conductivity curve plots of the Zn-GQD nanocomposite and the graphite materials (Table 2).

DISCUSSION

Percolation Modeling of Extracellular Electron Transfer

Percolation modeling was applied to simulate the critical phenomenon of conducting electrons from bacteria during extracellular electron transfer. In an MFC operation, this phenomenon represents the transfer of electrons in the interface between the extracellular matrix of bacteria and the electrodes. The redox reactions of bacterial metabolism produce the electrons deposited in the extracellular matrix of bacteria (Do et al., 2018). By definition, percolation concerns the transfer of information within clusters that form a link from boundary to boundary (Stauffer & Aharony, 2018). In the MFC process being simulated, the information refers to the electrons, while the boundaries refer to the extracellular matrix and the electrodes.

During the simulation, the electrodes were treated as random resistor networks composed of sites where percolation occurs (Mutiso & Winey, 2012). The cellular percolation models displayed in Figures 2, 3, and 4 show that the random resistor networks were arranged as a square lattice. Site percolation was used as this variant was applicable to the percolation of finite clusters (Aizenmann et al., 2015). In MFC applications, the electrodes carried finite length, width, and height (Do et al., 2018). The descriptions of conductivity offered by percolation models differed for each material largely because of their differences in critical percolation thresholds, dimensionality, and unit cell structures.

Critical Phenomenon Exhibited by the Electrode Materials

Cellular percolation models form a path at p_c because, at this threshold, the probability of generating percolating cells on the lattice is increased. Furthermore, the randomly generated percolating cells associate and form linkages and clusters that span from the top boundary to the bottom boundary of the percolating system's lattice, forming a path and allowing information to percolate (Aizenmann et al., 2015).

The sudden jump in the number and density of percolating cells on the lattice at p_c is attributed to the critical phenomenon that is the main subject observed in percolation theory (Ferraro et al., 2018). Percolation theory describes that a critical event or phenomenon occurs when a percolating system reaches its critical percolation threshold. The number of populations of percolating cells or units is sufficient to form clusters and linkages, allowing the system to percolate. This was highly evident and observable in the cellular percolation models of Zn-GQD, graphene, and graphite, as shown in Figures 2 (b), 3 (b), and 4 (b), respectively. At their p_c, the materials exhibited sudden jumps in the population of their percolating cells. These sudden jumps

led to the formation of the critical paths on which the percolating systems percolate. The magnitude of this critical event was most observable and extremely apparent in graphene because it had the highest p_c among the three materials due to its honeycomb lattice unit cell structure (Jacobsen, 2014). The probability of generating percolating cells, or percolation probability, increases at higher p_c values which explains why there is a more apparent sudden jump in the number of percolating cells at graphene's threshold (Aizenmann et al., 2015). These imply that the materials' unit cell structures and critical percolation thresholds are crucial factors that determine their percolation behavior. Hence, the degree or magnitude of the critical event varies from one material to another. These critical events manifest in the sudden jumps in the number of percolating cells in the percolating systems' lattices.

The upward trend observed in all $\theta(p)$ graphs of Figure 5 is explained by the positive correlation between $\theta(p)$ and p. The probability of percolation, $\theta(p)$, increases as the probability of an open site, p, increases. With more sites open and ready for percolation, the probability of forming spanning clusters increases as well. This is because there are more sites available for electrons to occupy and pass through (Steif, 2009).

It can be noticed in Figure 5 that the domain and range of $\theta(p)$ were constrained by the interval [0, 1]. The anchorage of percolation explains these properties in the language of statistical probability (Staufer & Aharony, 2018). Since statistical probabilities are quantified by the interval [0, 1], it follows that $\theta(p)$ exhibits the same intervals for its domain and range (Bluman, 2018).

Another notable observation in Figure 5 is how the $\theta(p)$ outputs of Zn-GQD and graphite were close to one another and were higher than the $\theta(p)$ outputs of graphene. This behavior may be attributed to the same dimensionality of Zn-GQD and graphite. Both Zn-GQD and graphite are 3D lattices (Protich et al., 2016; Li et al., 2016). Graphene, on the other hand, is 2D (Ray, 2015).

3D lattices were found to exhibit lower critical thresholds than 2D lattices. Therefore, the percolation probabilities for graphene rose earlier for graphite. The comparably lower critical thresholds of lattices with higher dimensions are mathematically explained by the decreasing trend of the numerical p_c approximations calculated by series expansions. In other words, numerical solutions to p_c decrease as the number of dimensions increases. Currently, no physical explanation exists to elaborate on this trend (Torquato & Jiao, 2013).

The comparison between Zn-GQD and graphite against graphene indicates that Zn-GQD and graphite electrodes percolate earlier than graphene electrodes. Consequently, the same trend is predicted to occur in their respective electrical conductivity curves. The cellular percolation models and percolation probability functions predict that Zn-GQD and graphite electrodes would demonstrate an earlier onset of conductivity in comparing electrical conductivity curves for the three-electrode materials.

Comparison of Electrical Conductivity Curves of the Electrode Materials

All of the electrical conductivity graphs displayed zero conductivity at $p < p_c$ (Figures 6, 7, and 8). This value is expected, for no spanning clusters are formed in the lattice of each material at this interval. Their percolating systems have yet to reach their critical thresholds where sites would suddenly form a bridge between the two boundaries of each percolating system (Steif, 2009). Due to a lack of a bridge, electrons could not pass through the interface between bacteria and electrodes. This result is confirmed by the cellular percolation models of each material displayed in Figures 2 (a), 3 (a), and 4 (a).

However, the electrical conductivity graphs continuously increased at $p \geq pc$ (Figures 6, 7, and 8). Zn-GQD starts conducting the earliest at $p = 0.199256$, followed by graphite at $p = 0.3701$

and graphene at p = 6970402. At this interval, their percolating systems crossed their critical thresholds. At least one spanning cluster exists within their lattices 100% of the time (Steif, 2009). This result is confirmed by the cellular percolation models of each material displayed in Figures 2 (b), 3 (b), and 4 (b). The result also confirms the ordering of the onset of conductivity predicted by the earlier percolation models. The $\sigma(p)$-graphs continuously increased, most likely because more spanning clusters are formed as p approaches 1. At $p = 1$, every possible cluster present in the lattice now spans from boundary to boundary (Steif, 2009).

Furthermore, all of the graphs were increasing exponentially at $p \geq pc$. This behavior is attributed to the power law used in the scaling equation (Mutiso & Winey, 2012). Based on Eq. 4.1, 4.2, and 4.3, the $\sigma(p)$ functions contained independent variables raised to the power greater than 1. The three-dimensional Zn-GQD and graphite used 2.00 as their exponent, while the two-dimensional graphene used 1.33. These values were gathered from mathematical simulations of percolation. While no physical explanation exists yet to elaborate on these values, exponents for higher dimensional lattices were always found to be relatively higher than to their lower dimensional counterparts according to computer approximations (Staufer & Aharony, 2018). However, based on the percolation probability functions, the exponential growth of conductivity may be attributed to the aggregation of spanning clusters as p approaches 1. More spanning clusters are available to serve as the pathway for the electrons to travel. The aggregated increase in the number of these pathways may have manifested in the electrical conductivity curves as an exponential increase.

Consequently, these values mathematically explain why the $\sigma(p)$ graphs of Zn-GQD and graphite look similarly quadratic and why the $\sigma(p)$ graph of graphene increases more abruptly. For the former, the scaling equations for Zn-GQD and graphite both used 2.00, hence the quadratic

shape. For the latter, lower exponents tend to produce steeper exponential growth for bases ranging from 0 to 1 (Dawkins, 2018). Since the (p - p_c) of Eq. 4.1, 4.2, and 4.3 were all constrained within the [0, 1] interval, the lower exponent of graphene provided a more abrupt growth.

Zn-GQD consistently posted higher conductivity than graphite. While graphene also demonstrated higher conductivity than graphite, the superiority was not as consistent as Zn-GQD. Graphite registered higher $\sigma(p)$ values for $0.3701 < p < 0.701$ before getting overtaken by graphene at $0.701 < p < 1$.

Analysis behind the Performance of the Zn-GQD Electrode

Based on the models, the consistency of the superior performance of Zn-GQD is attributed to the combination of its higher scaling constant and lower critical percolation threshold. The scaling constant and critical percolation threshold of Zn-GQD were 12.7 times higher and 1.86 times lower, respectively. On the other hand, graphene's relatively less consistent superior performance is attributed to its higher scaling constant but higher critical percolation threshold. The scaling constant and critical percolation threshold of graphene were 75.2 times higher and 1.88 times higher, respectively. Interestingly, the scaling constant of graphene was 5.92 times higher than that of Zn-GQD. This advantage of graphene was most apparent when its $\sigma(p)$ surpassed that of Zn-GQD at $0.828 < p \leq 1$.

Based on material properties, the consistency of the superior performance of Zn-GQD nanocomposite is attributed to the better electron capture and higher electron mobility of its quantum dot component. The electrodeposition of GQDs brings higher electron mobility in the nanocomposite electrode. The hexagonal rings of these nanostructures exhibit sp^2 hybridization in their carbon-carbon bonds. This results in the presence of conjugated π- bonds within the

hexagonal rings of graphene, which leads to the manifestation of aromaticity. Thus, electrons inside graphene rings are delocalized, similar to conductive metals. Wu et al. (2013) confirmed graphene's aromaticity using the Clar Sextet Rule. The delocalization of the electrons allows graphene to demonstrate excellent electrical and thermal conducting properties. The superior conductivity of graphene is largely attributed to the tendency of its electrons to behave like massless relativistic particles or massless Dirac fermions. Electrons in the aromatic ring of graphene are unusually accelerated spontaneously because of their interactions with the periodic potential of the honeycomb lattice (Berger, 2019). Additionally, the amplification of electron mobility is greater in GQDs due to characteristic quantum confinement. Quantum confinement is the phenomenon where a nanostructure material of size ten (10) nm or less causes its band gaps to increase and nearby excited electrons to be squeezed into an extent that reaches critical quantum measurement. GQDs are normally 5-7 nm in size, allowing them to possess special electronic behavior. As a result, electrons can freely move from atom to atom since the band gap energy, or the energy required for an electron to travel from the conduction band of one atom to the valence band of another is significantly lower than the kinetic energy possessed by the electrons that conform to quantum confinement (Wang et al., 2016).

However, the added electron mobility of quantum confinement comes with a drawback. Quantum confinement also has a detrimental effect on the electrical conductivity of the GQD components. The widened band gap of the GQD component of the nanocomposite may have been the cause of the lower peak electrical conductivity of individual Zn-GQD is relative to graphene at their peak (Figure 9) (Chen et al., 2019).

The Potential of Zn-GQD as an Advanced Electrode Material

Despite the shortcomings of Zn-GQD compared to graphene, the nanocomposite is deemed an ideal advanced electrode material for two main reasons. First, the percolation models predict that Zn-GQD trumps graphene and graphite with its balance between the early onset of conduction and decently high electrical conductivity (Figure 6). Zn-GQD exhibits the lowest critical threshold, which is responsible for the earliest formation of spanning clusters for electron pathways within its lattice. The formation of links at small probabilities may prove to be useful for conducting at low electrical outputs. Zn-GQD may be the optimal conductor for power sources whose voltages may not be sufficient enough to push significant percolation early on. An example of these systems is an MFC, whose voltage outputs are significantly limited by the voltage produced in bacterial respiration (Do et al., 2018). The free electrons generated in an MFC's anodic chamber are effectively captured by the Zn-GQD fragments scattered throughout the surface of the nanocomposite electrode. These fragments serve as individual percolating or conducting units that allow the captured electrons to easily percolate or be conducted through the Zn-GQD electrode despite the low voltage of the MFC because of their low percolation threshold (Lorenz et al., 2000). Meanwhile, the high conductivity of Zn-GQD arises when the percolating electrons become subjected to the GQDs' quantum confinement causing the electrons to jump-start and drastically magnifying the electrical conductivity of Zn-GQD (Wang et al., 2016).

Second, Zn-GQD offers excellent biocompatibility and good conductivity offered by its chemically inert GQD components. Excellent biocompatibility promotes bacterial colonization and attachment, while good conductivity allows for the efficient transfer of electrons to generate higher electrical current (Slate et al., 2018). The main candidates for electrode materials include metals and carbon-based materials. Metal electrodes display high conductivity but cannot allow

the attachment of bacteria. On the other hand, carbon-based electrodes show limited conductivity but allow convenient adherence of bacteria (Li et al., 2016). The Zn-GQD nanocomposite has the biocompatibility of carbon-based materials through the GQD layer, with the natural conductivity of zinc metals augmented by the increased electron mobility from the aromaticity and quantum confinement exhibited by GQDs.

In comparison to conventional carbon-based electrodes, the GQD layer on the zinc surface captures electrons from bacteria more effectively than graphite because of its higher surface area and planar aggregation. Flat planes enable more stable adherence of bacteria. Higher surface area leads to greater opportunities for extracellular electron transfer (Li et al., 2016).

The non-covalent bonding explained earlier between zinc, and GQDs allows the preservation of the characteristics of each individual component. Hence, the conductive properties of zinc metal are utilized along with the biocompatibility and conductivity of GQDs (Bagherzadeh & Farahbakhsh, 2015). This phenomenon is consistent with the reported ability of graphene to improve the energy conversion efficiency and power density of metal and metal oxide electrodes by approximately three-fold. This is because graphene, which contains carbon atoms, allows bacteria to adhere to inorganic metals. The modifications are usually done through the development of nanocomposite materials (e.g., Zn-GQD nanocomposite) (Li et al., 2016).

In the industrial setting, these benefits may be exploited in MFC applications such as bioenergy production, wastewater treatment, and biosensors (Do et al., 2018). These bacteria-powered operations will make good use of the predicted superiority of Zn-GQD over graphite and graphene in terms of optimum performance in conducting at low-to-mid end voltage outputs, biocompatibility, and corrosion resistance due to chemical inertness.

CONCLUSIONS

The respective percolation conductivities of Zn-GQD nanocomposite and graphite electrodes were successfully modeled through the construction of their cellular percolation models, percolation probability functions ($\theta(p)$), and electrical conductivity σ(S/m) curve plots. These models allowed the examination of the conductive phenomena exhibited by the materials. They also provided a new avenue to study the electrical conductivities of each material through percolation theory.

The models predicted that Zn-GQD is an ideal MFC electrode material for its balance between the early onset of conduction and decently high electrical conductivity. The electrode material was found to conduct at low probabilities of open sites and exhibit the highest electrical conductivity of the three materials for the longest duration across the interval.

For recommendations, future researchers are advised to create and study phenomenological models describing the possible inner workings of the electrode materials during extracellular electron transfer. Through this visualization, phenomenological models may provide more concrete physical interpretations of these factors that affect electrode performance. These interpretations may arise from revealing how percolation visually occurs on the internal structures of each material in real-time and how the electrodes exhibit biocompatibility during electron transfer. Original computational modeling programs and software may also be developed to provide more novel means of devising and constructing the percolation models.

Furthermore, experimental comparisons between Zn-GQD, graphene, and graphite in actual MFC applications are highly encouraged. These experiments may be used to confirm the electrical conductivity properties predicted by the percolation models of this study.

Lastly, future researchers are encouraged to conduct a cost-development analysis of Zn-GQD electrodes against the conventional and currently the best MFC electrode—graphite and graphene, respectively—to further explore the feasibility of the prospective advanced electrode material in industrial MFC applications.

REFERENCES

Aizenmann M., Kesten, H. & Newman, C. M. (2015). Uniqueness of the infinite cluster and continuity of connectivity functions for short- and long-range percolation. *Comm. Math. Phys.* 111, (2015), 505–532. http://doi org/10.1007/BF01219071/

Bagherzadeh, M., & Farahbakhsh, A. (2015). Surface functionalization of graphene. *Graphene Materials*, 25–65. https://doi.org/10.1002/9781119131816.ch2

Berger, M. (2019). *Graphene - All you need to know*. Nanowerk. https://www.nanowerk.com/what_is_graphene.php

Bluman, A. G. (2018). *Elementary statistics: A step by step approach*. McGraw-Hill Education.

Chen, Y., Chiang, W., Kurniawan, D., Yeh, P., Otake, K. & Kung, C. (2019). Impregnation of graphene quantum dots into a metal−organic framework to render increased electrical conductivity and activity for electrochemical sensing. *ACS Appl. Mater. Interfaces*, 11, 35319−35326, 2019. https://doi.org/10.1021/acsami.9b11447

Dawkins, P. (2018). *Algebra - Exponential functions.* https://tutorial.math.lamar.edu/classes/alg/expfunctions.aspx

Do, M., Ngo, H., Guo, W., Liu, Y., Chang, S., Nguyen, D., Nghiem, L., & Ni, B. (2018). Challenges in the application of microbial fuel cells to wastewater treatment and energy production: A mini review. *Science of The Total Environment, 639,* 910–920. https://doi.org/10.1016/j.scitotenv.2018.05.136

Ferraro, G., Moreno, A., Min, B., Morone, F., Ramirez, U., & Cervera, L. (2018). Finding influential nodes for integration in brain networks using optimal percolation theory. *Nature Communications 9*(1), 2274, 2018. https://doi.org/10.1038/s41467-018-04718-3

Jacobsen, J.L. (2014). High-precision percolation thresholds and Potts-model critical manifolds form graph polynomials. *Journal of Physics*, *47*(13). https://doi.org/10.1088/1751-8113/47/13/135001

Li, S., Cheng, C., & Thomas, A. (2016). Carbon-based microbial-fuel-cell electrodes: From conductive supports to active catalysts. *Advanced Materials*, *29*(8), 1602547. https://doi.org/10.1002/adma.201602547

Lilliefors, H. (2017). On the Kolmogorov-Smirnov Test for normality with mean and variance unknown. *Journal of the American Statistical Association*, *62*(318), 399-402. http://www.jstor.org/stable/2283970

Liu, Z., Bai, H., Luo, Y., Zhang, Q., & Fu, Q. (2017). Achieving a low electrical percolation threshold and superior mechanical performance in poly(L-lactide)/thermoplastic polyurethane/carbon nanotubes composites via tailoring phase morphology with the aid of stereocomplex crystallites. *RSC Advances*. https://doi.org/10.1039/c6ra27401c

Lorenz, C. D., May, R. & Ziff R.M. (2000). Similarity of percolation thresholds on the HCP and FCC lattices (PDF). *Journal of Statistical Physics*. 98 (3/4): 961–970. https://doi.org/10.1023/A:1018648130343

Mutiso, R. M., & Winey, K. I. (2012). Electrical conductivity of polymer nanocomposites. *Polymer Science: A Comprehensive Reference*, 327–344. https://doi.org/10.1016/b978-0-444-53349-4.00196-5

Protich, Z., Wong, P., & Santhanam, K. (2016). A new graphene composite with a high coulombic efficiency. *Journal of Power Sources*, *332*, 337–344. https://doi.org/10.1016/j.jpowsour.2016.09.118

Santoro, C., Kodali, M., Shamoon, N., Serov, A., Soavi, F., Merino-Jimenez, I., & Atanassov, P. (2019). Increased power generation in supercapacitive microbial fuel cell stack using Fe N C

cathode catalyst. *Journal of Power Sources*, 412, 416–424. https://doi.org/10.1016/j.jpowsour.2018.11.069

Slate, A. J., Whitehead, K. A., Brownson, D. A., & Banks, C. E. (2018). Microbial fuel cells: An overview of current technology. *Renewable and Sustainable Energy Reviews*, *101*, 60–81. https://doi.org/10.1016/j.rser.2018.09.044

Stauffer, D., & Aharony, A. (2018). Introduction to percolation theory 2nd Revised Edition. 1-3. https://doi.org/10.1201/9781315274386

Steif, J. (2009). *A mini course on percolation theory*. ResearchGate. htttps://www.researchgate.net/publication/251553930_A_mini-course_on_percolation_theory/

Torquato, S., & Jiao, Y. (2013). Effect of dimensionality on the percolation thresholds of various d-dimensional lattices. *Physical Review E*, *87*(3). https://doi.org/10.1103/physreve.87.032149

van der Marck, S. C. (1997). Percolation thresholds and universal formulas. *Physical Review E*, *55*(2), 1514–1517. https://doi.org/10.1103/PhysRevE.55.1514

Wang, S., Cole, I. S., Zhao, D., & Li, Q. (2016). Quasi-continuously tuning the size of graphene quantum dots via an edge-etching mechanism. *MRS Advances*, *1*(20), 1459–1467. https://doi.org/10.1557/adv.2016.198

Wolfram, S. (2011). *Percolation on a square grid*. Wolfram Demonstrations Project. https://demonstrations.wolfram.com/PercolationOnASquareGrid/

Wu, D., Gao, X., Zhou, Z., & Chen, Z. (2013). Understanding aromaticity of graphene and graphene nanoribbons by the Clar Sextet Rule. *Graphene Chemistry*, 29–49. https://doi.org/10.1002/9781118691281.ch3

ACKNOWLEDGMENTS

The student researchers acknowledge the efforts of their research adviser and research teacher, Mr. Francis M. Emralino and Ms. Michelle T. Manglicmot, respectively, for their extensive guidance and support throughout the study.

The student researchers also acknowledge their panelists for their helpful criticism and valuable insights for the betterment of the research project.

ABOUT THE AUTHORS

Jamme Omar A. Biscocho

Jamme Omar A. Biscocho is a ’21 graduate *With High Honors* from the Philippine Science High School – CALABARZON Region Campus. He earned awards for Best Presenter, Best Research Proposal, Best Research Paper, and Best Research Poster. He is currently pursuing BS Applied Physics at the University of the Philippines Diliman.

Ralph Calvin D. Almazan

Ralph Calvin D. Almazan is a ’21 graduate from the Philippine Science High School – CALABARZON Region Campus. He received an award for Best Research Proposal in 2019. He is currently taking BS Agricultural and Biosystems Engineering at the University of the Philippines Los Baños.

Francis M. Emralino

Francis Murillo Emralino is a Grade 12 Physics teacher at the Philippine Science High School – CALABARZON Region Campus. He holds a BS Applied Physics from the University of the Philippines Los Baños and is currently taking MS Physics at the De La Salle University Manila.

Michelle T. Manglicmot

Michelle T. Manglicmot is a research teacher at the Philippine Science High School – CALABARZON Region Campus. Previously, she served as a research associate at the UP Marine Science Institute and the Natural Sciences Research Institute. She finished her BS in Chemistry and MS in Environmental Science at the University of the Philippines Diliman.